Hydrogen−Exchange Stabilities of RNase T1 and Variants with Buried and Solvent−Exposed Ala → Gly Mutations in the Helix †

ARTICLE *in* BIOCHEMISTRY · DECEMBER 1999

Impact Factor: 3.02 · DOI: 10.1021/bi9919450 · Source: PubMed

Hydrogen-Exchange Stabilities of RNase T1 and Variants with Buried and Solvent-Exposed Ala → Gly Mutations in the Helix†

Beatrice M. P. Huyghues-Despointes,‡ Ulrike Langhorst,§ Jan Steyaert,§ C. Nick Pace,‡ and J. Martin Scholtz*,‡

Department of Medical Biochemistry and Genetics, Department of Biochemistry and Biophysics, Center for Macromolecular Design, Texas A&M University, College Station, Texas 77843, and Dienst Ultrastructuur, Vlaams Interuniversitair instituut voor Biotechnologie, Vrije Universiteit Brussel, Paardenstraat 65, B-1640 Sint-Genesius-Rode, Belgium

Received August 19, 1999; Revised Manuscript Received October 8, 1999

ABSTRACT: Hydrogen-exchange rates were measured for RNase T1 and three variants with Ala → Gly substitutions at a solvent-exposed (residue 21) and a buried (residue 23) position in the helix: A21G, G23A, and A21G + G23A. These results were used to measure the stabilities of the proteins. The hydrogen-exchange stabilities (ΔG_{HX}) for the most stable residues in each variant agree with the equilibrium conformational stability measured by urea denaturation (ΔG_U), if the effects of D_2O and proline isomerization are included [Huyghues-Despointes, B. M. P., Scholtz, J. M., and Pace, C. N. (1999) *Nat. Struct. Biol. 6*, 210−212]. These residues also show similar changes in ΔG_{HX} upon Ala → Gly mutations ($\Delta\Delta G_{HX}$) as compared to equilibrium measurements ($\Delta\Delta G_U$), indicating that the most stable residues are exchanging from the globally unfolded ensemble. Alanine is stabilizing compared to glycine by 1 kcal/mol at a solvent-exposed site 21 as seen by other methods for the RNase T1 protein and peptide helix [Myers, J. K., Pace, C. N., and Scholtz, J. M. (1997) *Proc. Natl. Acad. Sci. U.S.A. 94*, 3833−2837], while it is destabilizing at the buried site 23 by the same amount. For the A21G variant, only local NMR chemical shift perturbations are observed compared to RNase T1. For the G23A variant, large chemical shift changes are seen throughout the sequence, although X-ray crystal structures of the variant and RNase T1 are nearly superimposable. Ala → Gly mutations in the helix of RNase T1 at both helical positions alter the native-state hydrogen-exchange stabilities of residues throughout the sequence.

It has been known for many years that the hydrogen exchange of amide groups in a protein with solvent water can vary by many orders of magnitude (*1*). A surface residue exchanges readily with the solvent, while an interior and/or hydrogen-bonded residue may not exchange unless the protein unfolds to a partially or globally unfolded form. A general two-step model for hydrogen exchange can be described by

$$(\mathrm{N{-}H\cdots O{=}C})_{cl} \underset{k_{cl}}{\overset{k_{op}}{\rightleftharpoons}} (\mathrm{N{-}H})_{op} \xrightarrow{k_{rc}} \mathrm{N{-}D} \qquad (1)$$

where an amide group undergoes structural opening (k_{op}) and closing (k_{cl}) to an exchange-competent form, $(N-H)_{op}$ (*1*). From this state, an amide group readily exchanges with solvent with an intrinsic rate constant for exchange (k_{rc}). Under EX2 conditions where $k_{cl} \gg k_{rc}$, the observed rate constant for exchange, k_{ex}, is $K_{op}k_{rc}$, where K_{op} is the equilibrium constant for structural opening ($K_{op} = k_{op}/k_{cl}$). Thus, the free-energy change for structural opening, ΔG_{HX}, can then be calculated with

$$\Delta G_{HX} = -RT \ln(k_{ex}/k_{rc}) \qquad (2)$$

using the measured k_{ex} values and the k_{rc} values based on peptide models of Bai et al. (*2*).

How the hydrogen-exchange rates of individual groups relate to the global conformational stability and the folding process is less clear. Several groups have explored this relationship by measuring the response of hydrogen-exchange rates to protein denaturant (*3*−*9*), temperature (*4*, *10*, *11*), pressure (*12*), or mutation (*13*−*15*). The analysis of the dependence of external perturbants typically requires that the exchange rate constants be converted to stabilities using eq 2. Thus, the k_{rc} for unstructured peptides must be used. In contrast, the change in stability upon mutation, $\Delta\Delta G_{HX}$, can be obtained directly from the hydrogen-exchange rate constants by

$$\Delta\Delta G_{HX} = (\Delta G_{HX})_{WT} - (\Delta G_{HX})_{mutant} = -RT \ln(k_{ex})_{WT}/(k_{ex})_{mutant} \qquad (3)$$

for all residues except at the mutation site and for the residue $(i + 1)$ from this site where the k_{rc} values do not cancel.

Many studies suggest that the most stable residues exchange through the unfolded protein ("global"), the residues with intermediate stabilities exchange by fluctuations in the native state ("local") or by partial unfolding ("subglobal"), and the least stable residues exchange directly with

† Supported by Grants from the National Institutes of Health (GM37039 to C.N.P. and GM52483 to J.M.S.) and the Robert A. Welch Foundation (A-1060 to C.N.P. and A-1281 to J.M.S.). J.M.S. is an American Heart Association Established Investigator and C.N.P. is supported by the Tom and Jean McMullin Professorship.

* To whom correspondence should be addressed. Phone: (409) 845-0828. Fax: (409) 847-9481. E-mail: jm-scholtz@tamu.edu.

‡ Texas A&M University.

§ Vrije Universiteit Brussel.

10.1021/bi9919450 CCC: $18.00
Published on Web 11/20/1999

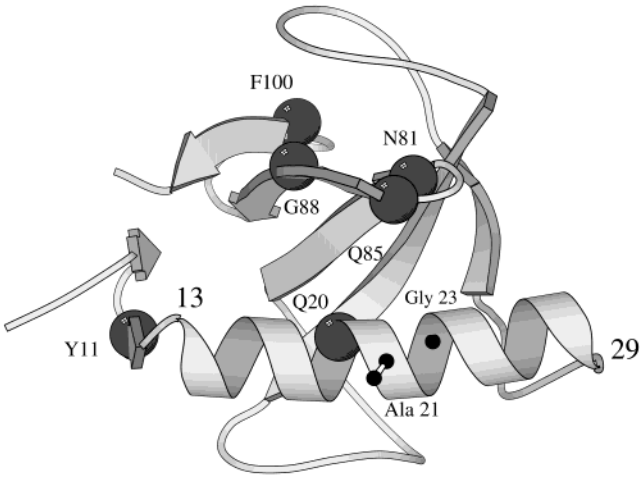

FIGURE 1: Ribbon diagram of RNase T1 based on the crystal structure determined by Martinez-Oyanedel et al. (*62*) and created using MOLSCRIPT (*63*). The NH groups of the six most stable residues in all four variants are in CPK. Mutations are in the helix at the solvent-exposed residue 21 and the buried residue 23.

the solvent in the native state (*13*, *15*, *16*). One interesting question that remains is whether the global residues identified by using eqs 2 or 3 are the same.

The conformational stabilities calculated by hydrogen-exchange rate constants of the most protected residues using eq 2 are often greater than the global conformational stability measured by traditional methods. This has led to controversies about the nature of the exchange process of these residues and whether the peptide-based k_{rc} values adequately model hydrogen exchange in proteins (*17*−*19*). Only recently has this difference been shown to result from the D_2O solvent isotope effect and proline isomerization for many proteins (*20*). There are two relevant points to consider. First, proteins may be more or less stable in D_2O than in H_2O. It is important therefore to only compare hydrogen exchange and equilibrium unfolding stabilities that have been determined in D_2O. Second, the cis/trans conformation of a Xaa−Pro bond in a protein is different under native-state conditions than under equilibrium unfolding conditions. The Xaa−Pro bond in the native state is primarily in one conformation, while the Xaa−Pro bond in the equilibrium unfolded state is a mixture of cis and trans conformations. The unfolded protein contains 6−38% of the cis conformation depending on the identity of Xaa (*21*). Since native-state hydrogen exchange occurs much faster than the time it takes for proline isomerization, a difference in free energy between hydrogen-exchange and traditional measurements equaling the free energy of proline isomerization is observed. When these two effects are included, it appears that the most protected backbone amide hydrogens exchange only after global unfolding and the exchange of the unfolded state is modeled well by the peptide-based k_{rc} values of Bai et al. (*2*). Thus, the conformational stability can be determined adequately from hydrogen-exchange rates using eq 2 for the most stable residues in most proteins.

RNase T1 is used here as a model system to examine hydrogen-exchange stabilities as a function of mutation. RNase T1 is a small (104 residues) $\alpha + \beta$ protein where the β-sheets pack against a 17 residue α-helix to form the hydrophobic core (Figure 1). It shows reversible two-state unfolding with denaturant and temperature. It has been shown previously that RNase T1 is a good protein to measure the helix propensities of amino acids in a natural system. The sequence of the helix (residues 13−29) is SSDVSTAQ**A**A**G**-YKLHED. Alanine 21 is a completely exposed residue in the center of the helix and seems to make no contacts with other residues. Glycine 23 is on the buried face of the helix and packs against β-sheets 3 and 4 of the protein. A peptide with the wild-type sequence shows a CD spectrum characteristic of a random-coil conformation. However, if glycine 23 is replaced with alanine, the resulting peptide is helical. This mutation allowed Myers et al. (*22*−*24*) to investigate helix propensities of amino acids at site 21 in RNase T1 and in a helical peptide of identical sequence.

We present here an analysis of NMR chemical shifts of the variants and the X-ray crystal structure of G23A. The native-state hydrogen exchange of RNase T1 and three variants (A21G, G23A, and A21G + G23A) are then measured and compared to equilibrium unfolding measurements to identify global-exchanging residues. Last, we compare the effect of mutation on the global residues and nonglobal residues.

EXPERIMENTAL PROCEDURES

Mutagenesis and Protein Purification. RNase T1 and the Ala → Gly variants were produced previously (*22*) by site-directed mutagenesis using the polymerase chain reaction (*25*). The proteins were expressed in the periplasmic space of *Escherichia coli* by using the pHN1+ and PJF118EH expression vectors for G23A and A21G + G23A variants and the pMC−RT1 vector for RNase T1 and the A21G variant. The ^{15}N-labeled proteins were produced by transforming the plasmids in the *E. coli* strain MQ by electroporation. The cells were grown first in unlabeled M9 minimal media to a maximum density and then spun down and resuspended in M9 minimal media with $^{15}N-NH_4Cl$. Protein expression was induced with 1 mM IPTG, and the cells were harvested after a single doubling period. The mutants were purified as described previously (*26*). SDS−polyacrylamide gel electrophoresis was used to confirm the protein purity. All mutations resulted in stable, active ribonucleases.

Urea Denaturation. The conformational stability of RNase T1 and the variants was determined in D_2O using urea denaturation as monitored by intrinsic tryptophan fluorescence. The deuterated urea (Sigma Ultrapure or Nacalai Tesque) was prepared by several cycles of lyophilization from D_2O. The stock solutions of urea were prepared fresh daily and their concentrations were determined by refractive index measurements (*27*). Protein stock solutions were prepared in D_2O in 50 mM sodium acetate at pD 7.4 or 7.7 for RNase T1 and pD 7.4 for the variants. pD is the addition of 0.4 to the pH meter reading when the sample is in D_2O (*28*). After equilibration of protein samples for 16 h at 25 °C, urea denaturation curves were determined by measuring the intrinsic tryptophan fluorescence intensity at 320 nm after excitation at 278 nm with an SLM AB2 or SLM 8100 spectrofluorometer. A minimum of three denaturation curves was performed for each variant.

Hydrogen Exchange by NMR Spectroscopy. Samples were prepared by dissolving the protein (1.5−2.0 mM) in H_2O and 50 mM sodium acetate and allowed to equilibrate at 25 °C for 16 h. The protein sample was then exchanged into

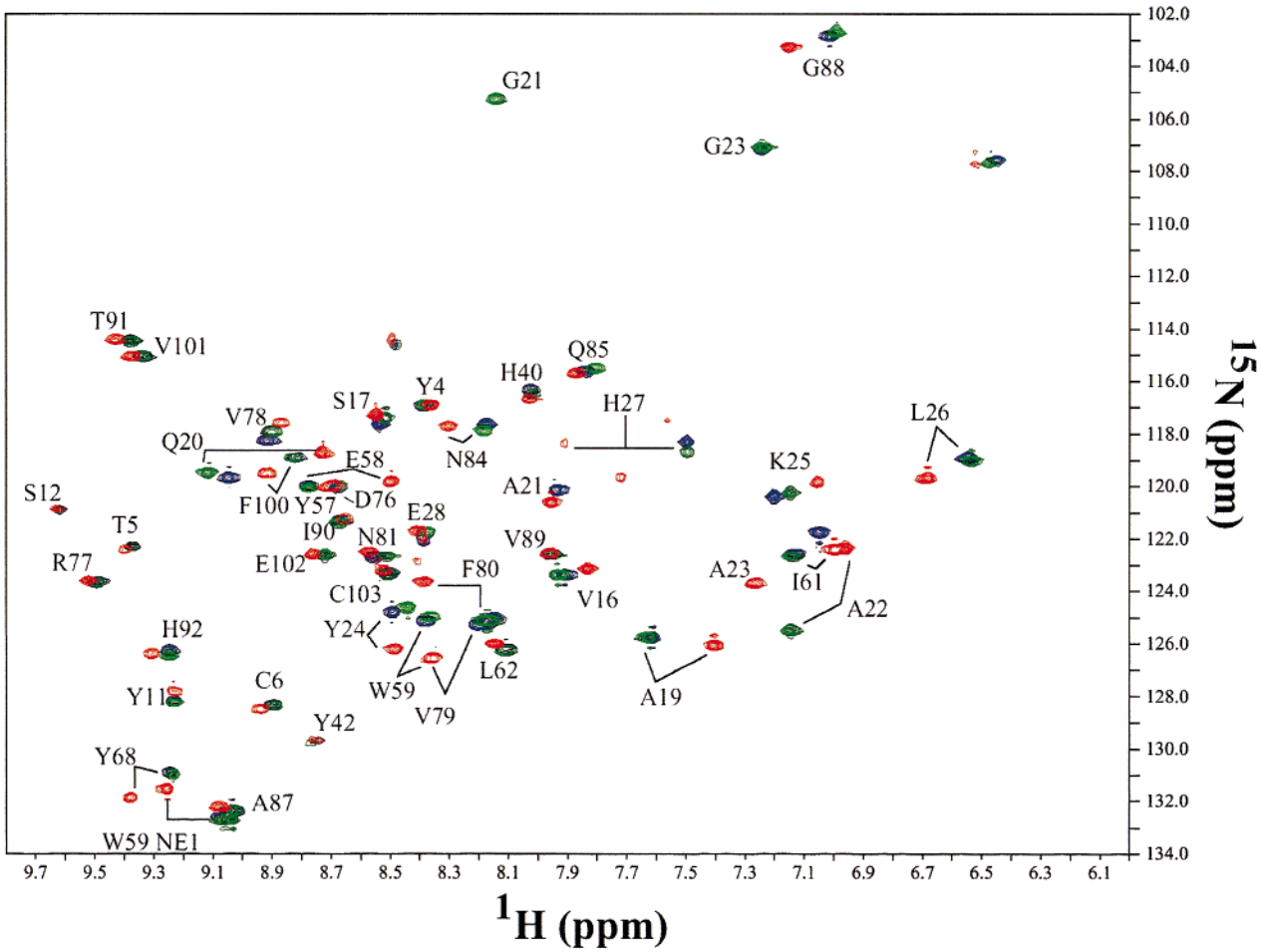

FIGURE 2: Overlay of ^{15}N-^{1}H HSQC spectra of RNase T1 (blue), the A21G (green), and the G23A (red) variants.

D_2O and 50 mM deuterated sodium acetate (Isotec) using a spin column (Isolab Inc.). The protein sample was immediately placed in the NMR spectrometer with the probe temperature at 25 °C. NMR spectra were collected over time with a 500 MHz Varian Unity spectrometer, equipped with a triple resonance probe. ^{15}N-^{1}H HSQC spectra were recorded with 4−8 transients of 1024 data points and 256 T_1 increments with sweep widths of 7002.8 and 2080 Hz in the ^{1}H and ^{15}N dimensions. Water suppression by presaturation was used. ^{15}N-^{1}H HSQC spectra were obtained over various time intervals (2 weeks to 6 months depending on the pH and the stability of the variant). The spectra were processed by nmrPipe and visualized by nmrDraw (*29*).

Cross-peak intensities of the ^{15}N-^{1}H HSQC spectra for each variant were measured by volume integration using nmrDraw. Peak intensities were then fit to a single-exponential function, $A = A_0[e^{(-kt)}] + C$, where C is baseline noise of a particular sample. The errors of hydrogen-exchange free energies did not exceed 0.3 kcal/mol, determined using the 67% confidence interval on the error of the rate constants calculated by NONLIN (*30*). The errors were the largest for residues whose hydrogen-exchange rates were either very fast or very slow. The intrinsic exchange rates for residues in random coil peptides were calculated (*2*), using the appropriate temperature and pH with corrections for the known pK_a values for the histidine residues (*31*).

Since limited chemical shift perturbations for A21G variant were seen, the assignments of the ^{15}N-^{1}H HSQC spectra were made by direct comparison to RNase T1 spectrum (*32*). Standard sequential assignment techniques were used to assign ambiguous peaks in the G23A and G23A + A21G variants. Two-dimensional homonuclear NOESY (t_m = 70 ms), TOCSY (70 ms), and COSY spectra were used for assignments, using the published RNase T1 spectra as a reference (*33*).

Crystallization, Structure Determination, and Refinement of RNase T1 G23A. We obtained crystals of G23A mutant in complex with the specific inhibitor 2′-GMP using the hanging drop technique aided by macroseeding. Data were collected from single needle-shaped crystals with typical dimensions 0.60 × 0.04 × 0.03 mm using a MAR Image Plate detector and a RIGAKU Rotating anode X-ray generator operated at 40 kV, 90 mA. The data were indexed as orthorhombic resulting in space group $P2_12_12_1$, integrated using DENZO (*34*) and subsequently scaled and merged using SCALEPACK (*35*). The CCP4 program TRUNCATE (*34*) was used to convert intensities into structure factors.

The structure of the G23A mutant was solved starting from the refined coordinates of the isomorphous wild-type structure PDB entry 1rga (*36*) stripped of all its solvent and inhibitor molecules. Refinement was done with X-PLOR version 3.851 (*37*) using all reflections in the resolution range 15.0−1.95 Å. The refinement was started with a slow cool stage to reduce bias toward the starting model. A bulk solvent correction was calculated after each rebuilding session. When no further errors in the protein region of the electron density

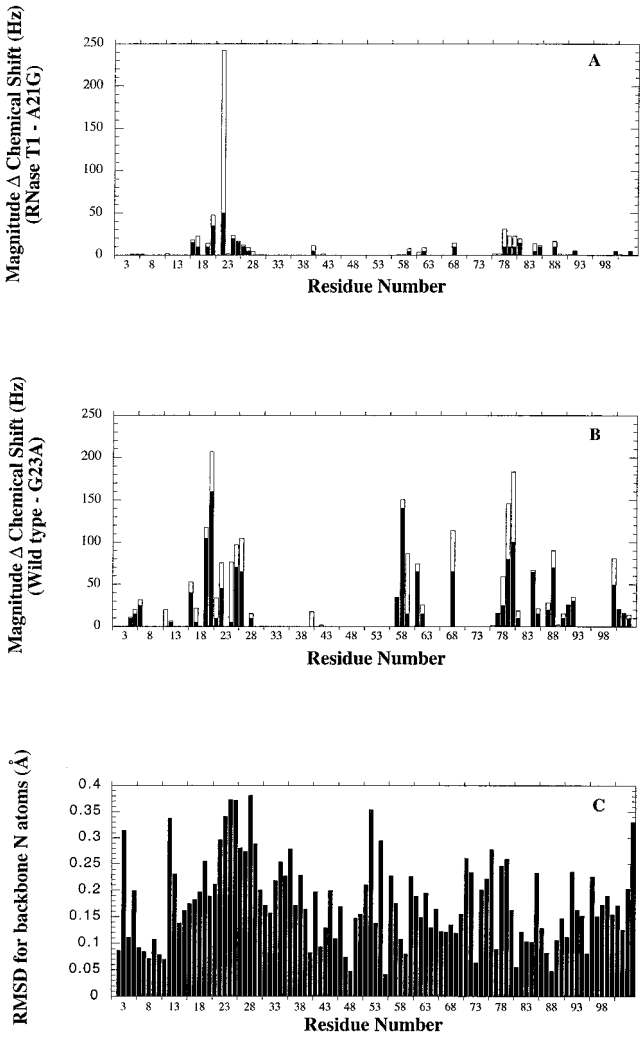

FIGURE 3: Magnitude difference in chemical shift in hertz for ^{1}HN (solid bars) and ^{15}N (open bars) between RNase T1 and the A21G (panel A) or G23A variants (panel B). The NH RMSD between RNase T1 (PDB entry number 5bu4) (*40*) and the G23A variant (panel C).

map could be found, the inhibitor 2′-GMP and a calcium ion were built into the electron density map. Water molecules were included if (1) they could be identified as peaks of at least 3σ in $F_o - F_c$ maps, (2) they reappeared after refinement in $2F_o - F_c$ maps of at least 1σ, (3) they made at least one reasonable hydrogen bond to a protein or inhibitor atom, and (4) they showed no van der Waals clashes with any protein or inhibitor atom or with a previously identified water molecule.

The stereochemical quality of the refined structure was verified with PROCHECK (*38*). The refined model coordinates have been deposited in the protein databank (*39*) and given the accession code 1rhl.

RESULTS

Chemical Shift and Crystal Structure Analysis. A comparison of ^{15}N-^{1}H HSQC spectra of RNase T1 with the A21G and G23A variants is shown in Figure 2, and the changes in chemical shift (in hertz) as a function of residue position for the single mutants relative to RNase T1 are shown in Figure 3. The chemical shifts of residues in the solvent-exposed A21G variant (green) and RNase T1 (blue) are nearly identical, except near the mutation site (Figure 2). The change in chemical shift of Ala22 is largest, and smaller changes for other residues in the helix (Gln20, Tyr24, Lys25, and His27) are observed. Residues outside of the helix are essentially not affected by the A21G mutation.

In contrast, the cross-peaks for the G23A variant (red) display large changes in chemical shifts compared to RNase T1 (blue) for residues throughout the entire protein (Figure 2). In the helix, the chemical shifts of residues that are (i,$i\pm4$) (Ala19 and His27) and (i,$i\pm3$) (Gln20 and Leu26) from the substitution site show the largest changes (Figure 3B). The β-strand residues near site 23, such as Trp59, Phe80, Tyr57, and Tyr68, and their neighboring residues (Val79, Val78, and Glu58) are also affected by the mutation. We observe small changes in chemical shift for residues outside the region of the mutation.

We also obtained the X-ray crystal structure of the G23A variant to compare the structure to RNase T1. The crystallization conditions for G23A were identical to the conditions used to determine the RNase T1 wild-type structure (*40*). The crystallographic data for the G23A variant are shown in Table 1, and the RMSD (Å) for the backbone amide nitrogens is shown in Figure 3C. The deviation in the overall backbone amide nitrogen RMSD is 0.2 Å, and the RMSD for all atoms in the backbone is 0.42 Å. The changes in NMR chemical shifts and in backbone nitrogen RMSD are consistent; variations in G23A are seen mainly in the helix and near the mutation site in β-sheets 3 and 4. The chemical shift changes are, however, more pronounced and sensitive to the mutation. The structure of G23A is nearly super-

Table 1: Crystallographic Data for RNase T1 G23A

crystallization conditions	10 mg/mL protein
hanging drop	50 mM sodium acetate, pH 4.2
microseeding	2 mM 2′GMP
	2 mM $CaCl_2$
	50% MPD[a]
space group	$P2_12_12_1$
unit cell	
a	40.44 Å
b	48.23 Å
c	50.95 Å
no. of measured reflections	50 578
no. of unique reflections	7378
working set	6563
test set	691
completeness	96.2%
redundancy	6.8%
resolution	15.00−1.95 Å
R_{merge} overall[b]	0.126 (0.475)
I/σ_I overall[b]	10.7 (3.3)
R-factor overall[b]	0.164 (0.222)
R_{free}-factor overall[b]	0.208 (0.232)
Ramachandran	
most favored	94.3%
additionally allowed	5.7%
generously allowed	0.0%
disallowed	0.0%
RMS	
bond lengths	0.006 Å
bond angles	1.556°
dihedral angles	24.928°
improper angles	1.064°
no. of water molecules	88
no. of multiple conformations	2

[a] MPD, 2-methyl-2,4-pentanediol. [b] Parameters in parentheses are given for the highest resolution shell.

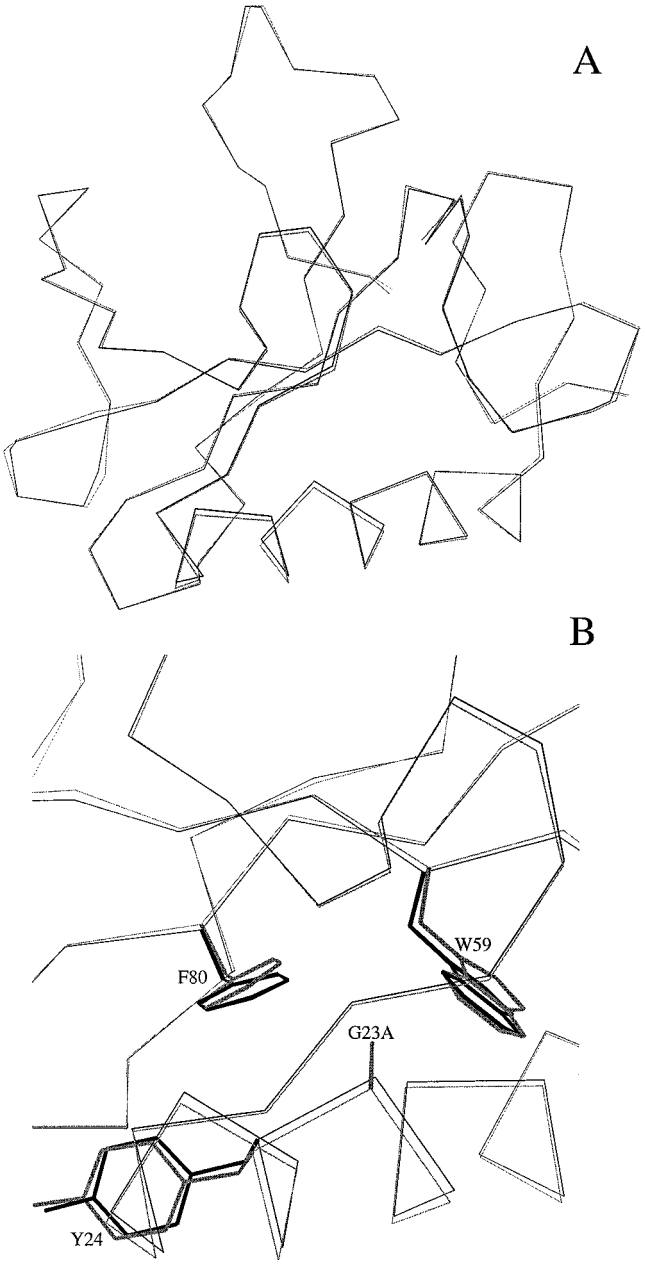

FIGURE 4: Structural alignments of G23A (gray) and RNase T1 (black) (PDB entry number 5bu4) (*40*) in panel A. Panel B shows more detail near the G23A site. Side chains that rearrange with the mutation are included.

imposable with the RNase T1 structure as shown by the backbone alignments of RNase T1 and the G23A variant in Figure 4A. Small differences are observed in the backbone helical residues near the mutation site and in side-chain conformations of Trp59, Phe80, and the C-terminal residues of the helix (Figure 4B).

Urea Denaturation. The effect of mutations on the conformational stability of RNase T1 was determined using equilibrium urea denaturation in D_2O. The denaturation curves were analyzed by assuming two-state unfolding and the linear extrapolation method

$$\Delta G = \Delta G_U(D_2O) - m[\text{urea}] \quad (4)$$

where the *m*-value describes the dependence of free energy of unfolding on denaturant concentration and $\Delta G_U(D_2O)$ is an estimate of the conformational stability in D_2O in the absence of urea (*27*, *41*). The equilibrium conformational stabilities (ΔG_U) and parameters characterizing the urea denaturation curves at pD 7.4 and 25 °C are given in Table 2. ΔG_U was also determined at pD 7.7 for RNase T1 for comparison with hydrogen-exchange studies. All variants are destabilized compared to RNase T1. The A21G and G23A variants are destabilized by 1.1 and 1.2 kcal/mol, respectively, and the A21G + G23A variant is destabilized by 2.2 kcal/mol.

Table 2: Conformational Stabilities of RNase T1 and Three Variants Determined by urea Denaturation[a]

RNase T1[b]	$D_{1/2}$ (M)[c]	*m* (kcal/mol M)[d]	ΔG_U (kcal/mol)[e]
WT pD = 7.4	6.4_2	1.25	8.2
(A21 G23) pD = 7.7	6.1_5	1.23	7.9
A21G (**G21** G23)	5.5_3	1.30	7.1
G23A (A21 **A23**)	5.4_9	1.26	7.0
A21G+G23A **(G21 A23)**	4.7_0	1.37	6.0

[a] The samples were buffered in D_2O with 50 mM sodium acetate at pD 7.4 and 25 °C. [b] The four RNase T1 variants used in this study. Residues at position 21 and 23 in each variant are represented in parentheses. The boldfaced residues are the sites mutated. [c] Concentration of urea where the protein is half-denatured. Error is estimated to be ±0.1 M. [d] Linear dependence of ΔG on urea concentration (eq 4). [e] Global free energy of unfolding, calculated using the product of $D_{1/2}$ and the average *m*-value for all mutants (1.28 ± 0.07 kcal/mol M) (eq 4). The error estimated as ±0.5 kcal/mol.

Table 3: Change in Stability upon Ala → Gly Mutations in the Helix of RNase T1 at pD 7.4

solvent-exposed Ala → Gly	$\Delta\Delta G_U$[a] (kcal/mol)
WT−A21G	1.1_4
G23A−A21G+G23A	1.0_1
buried Ala → Gly	
G23A−WT	-1.1_9
A21G+G23A−A21G	-1.0_6

[a] The change in stability upon mutation is determined by the product of the difference in $D_{1/2}$ and the average m-value for all mutants. Positive $\Delta\Delta G_U$ values indicate that the Ala-containing protein is more stable. The change in stability upon mutation where both the urea denaturation curves were measured at pD 7.4.

The differences in the conformational stabilities, $\Delta\Delta G_U$, for the solvent-exposed and buried Ala → Gly mutations in the helix of RNase T1 are shown in Table 3. Alanine at exposed site 21 is stabilizing by 1.0 kcal/mol compared to glycine. In contrast, alanine at buried site 23 is destabilizing by 1.1 kcal/mol compared to glycine. The additivity of the $\Delta\Delta G_U$ of the single Ala → Gly mutations in the double variant suggests that the two sites behave independently (*42*).

It is important to note that the variants are more stable in D_2O than in H_2O. The D_2O solvent isotope effect causes a 1.4 kcal/mol increase in stability for RNase T1 as determined by urea denaturation (*20*). The *m*-values (Table 2) and the changes in stabilities between variants are the same within error in D_2O and H_2O. The average *m*-value in D_2O is 1.28 ± 0.07 kcal/mol M. This is close to the value of 1.21 ± 0.07 kcal/mol M observed by Myers et al. (*22*) for the set of 20 RNase T1 variants at position 21 (A21X) measured in H_2O.

Hydrogen Exchange. The hydrogen-exchange rate constants were measured for RNase T1 and the three variants

Table 4: Hydrogen-Exchange Stabilities for RNase T1 Variants[a]

			ΔG_{HX} (kcal/mol)			
residue	structure	HB acceptor	wild-type	A21G	G23A	A21G+G23A
Y4	βA	Y11 O	9.1	8.3	8.3	7.7
T5	βA	T104 Oxt	6.8	6.4	6.5	5.9
C6	βA	N9 O	7.9	7.6	7.5	7.0
Y11	βB	Y4 O	**10.1**	**9.3**	**9.3**	**8.4**
S12	βB	D15 Oδ2	*c*	6.2	*c*	*c*
V16	helix	S12 O	8.2	7.5	7.5	7.0
S17	helix	S13 O	7.5	7.0	7.1	6.6
A19	helix	D15 O	8.9	8.3	8.0	7.5
Q20	helix	V16 O	**10.4**	**9.2**	**9.1**	**8.3**
A/G21	helix	S17 O	**10.2**	7.8	**9.1**	7.8
A22	helix	T18 O	9.2	7.7	8.1	6.9
G/A23	helix	A19 O	**10.1**	9.0	**9.6**	**8.8**
Y24	helix	Q20 O	**10.2**	8.9	8.9	**8.0**
K25	helix	A21 O	6.9	6.1	5.6	*c*
L26	helix	A22 O	7.4	6.8	6.1	5.6
H27	helix	Y24 O	6.4	6.2	*c*	*c*
E28	helix	Y24 O	6.1	5.9	5.8	5.7
H40	β1	E58 O	9.6	**9.3**	**9.1**	**8.7**
Y42	β1	Y56 O	*c*	5.5	*c*	*c*
Y57	β2	F80 O	*b*	*b*	**9.1**	**8.3**
E58	β2	H40 O	*b*	*b*	8.1	7.4
W59	β2	V78 O	**10.3**	**9.5**	*b*	*b*
I61	β2	D76 O	9.7	8.2	7.7	6.6
L62	β2		7.3	6.9	6.6	6.3
Y68	loop		5.8	5.4	5.5	5.5
D76	β3		*c*	5.4	*c*	*c*
R77	β3	I90 O	**10.3**	9.0	**9.1**	**8.5**
V78	β3	W59 O	**10.0**	8.9	8.8	**8.1**
V79	β3	G88 O	*b*	*b*	*b*	*b*
F80	β3	Y57 O	*b*	*b*	**9.0**	**8.2**
N81	β3	Q85 O	**10.8**	**9.9**	**9.7**	**9.0**
N84	β4	N81 O	9.1	8.8	8.2	7.9
Q85	β4	N81 Oδ1	**10.5**	**9.6**	**9.4**	**8.7**
A87	β4	V79 O	**10.4**	**9.6**	8.9	**8.2**
G88	β4	V79 O	**10.7**	**9.3**	**9.4**	**8.6**
V89	β4		6.4	6.0	6.0	5.7
I90	β4	R77 O	9.6	8.6	8.3	7.3
T91	β4	V101 O	9.6	8.5	8.5	7.9
H92	β4	A75 O	9.8	**9.4**	**9.2**	**8.4**
F100	β5	E46 Oϵ2	**10.7**	**9.6**	**9.5**	**8.7**
V101	β5	T91 O	9.1	8.6	8.3	7.7
E102	β5		5.4	5.1	5.0	4.7
C103	β5	V89 O	8.2	8.0	7.9	7.6
	ΔG_U^{*d}		**10.4**	**9.6**	**9.5**	**8.5**

[a] The experiments were performed at 25 °C; the samples were buffered with 50 mM sodium acetate,*d3* at pD 7.4 in D_2O, except for RNase T1 where the pD was 7.7. Hydrogen-exchange stabilities for residues in boldface appear to exchange primarily from the globally unfolded protein. [b] Values not determined because of spectral overlap. E58 overlapped with Y57 for RNase T1 and the A21G variants. V79 overlapped with W59 in the G23A and variants and with F80 in RNase T1 and A21G variant (see Figure 2). [c] Rates too fast to measure by hydrogen-exchange experiments. [d] The ΔG_U (Table 2) corrected for proline isomerization using the Xxx−Pro estimates from pentapeptides (*20*, *21*) for the four prolines in RNase T1. The correction for proline isomerization is 2.53 kcal/mol for RNase T1. The error in ΔG_U^* is estimated to be ±0.5 kcal/mol.

(see Supporting Information Table 1). The ΔG_{HX} values for the 42 measurable amide protons were determined using eq 2 and the k_{rc} values from model peptide data (*2*). The ΔG_{HX} values are given in Table 4. The hydrogen-exchange rates of RNase T1 and the variants obey EX2 behavior at pD 7.4−7.7, as discussed previously (*11*, *20*).

The ΔG_{HX} values for the most stable residues in all four variants are considerably larger than the corresponding ΔG_U values (compare stabilities in Tables 2 and 4). The ΔG_{HX} values are not directly comparable to ΔG_U values measured by urea denaturation, unless a correction for cis ↔ trans proline isomerization is included, as summarized above and discussed previously (*10*, *20*). RNase T1 has two cis prolines (Tyr−Pro39 and Ser−Pro55) and two trans prolines (Trp−Pro60 and Ser−Pro73). Therefore, the total correction for the Xaa−Pro isomerization effect on RNase T1 and the variants is 2.53 kcal/mol [determined from Table 2 in Huyghues-Despointes et al. (*20*) using data from Reimer et al. (*21*)]. If we add this contribution to the ΔG_U values (denoted as ΔG_U^*), we find good agreement between ΔG_U^* and ΔG_{HX} for the most stable residues. The ΔG_{HX} values that agree within error (± 0.5 kcal/mol) to ΔG_U^* are boldfaced in Table 4.

The effect of the Ala → Gly mutations on stability for each measurable residue is shown in Figure 5. We determined

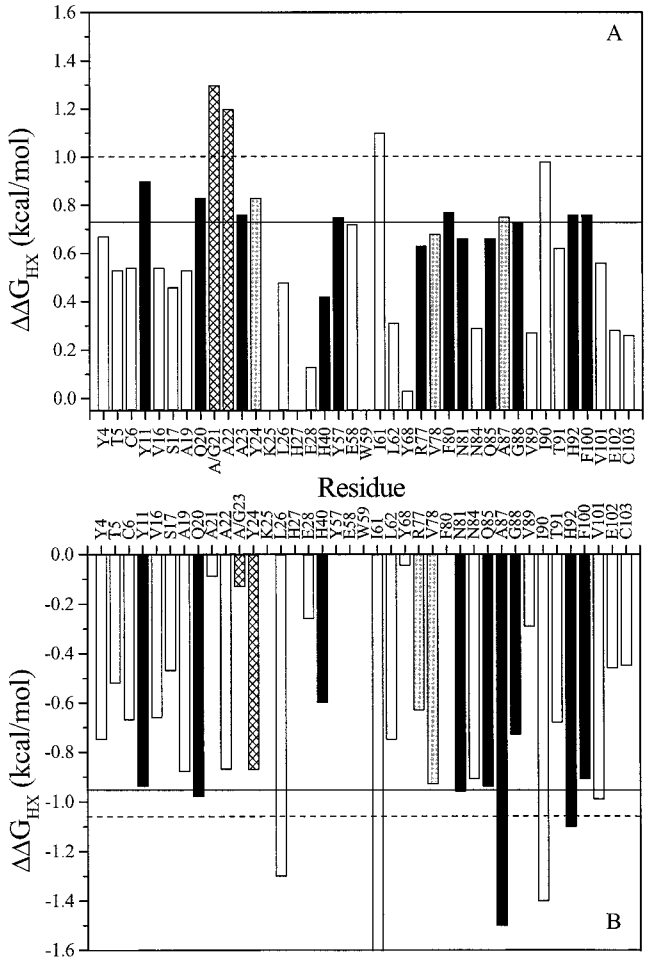

FIGURE 5: $\Delta\Delta G_{HX}$ values for the Ala → Gly mutations determined using eq 3 for all residues except for the mutated and the $(i + 1)$ residue. (A) The effects of an Ala → Gly mutation at the solvent-exposed residue 21. G23A and A21G + G23A variants are compared. (B) The effects of an Ala → Gly mutation at the buried residue 23. A21G + G23A and A21G variants are compared. Positive $\Delta\Delta G_{HX}$ values indicate that the alanine-containing protein is more stable. We compare only variants whose exchange measurements were made at pD 7.4 and 25 °C. Solid bars, residues which have global ΔG_{HX} values in both variants; gray bars, residues which have global ΔG_{HX} values in only one variant; white bars, residues that are nonglobal in both variants; hatched bars, the mutated and the $(i + 1)$ residues. The k_{rc} values were used as shown in eq 2 to determine $\Delta\Delta G_{HX}$ for residues represented by hatched bars. Solid line, average $\Delta\Delta G_{HX}$ value for the global residues. Dashed line, $\Delta\Delta G_U$ value by urea denaturation.

$\Delta\Delta G_{HX}$ using eq 3 for all residues except at the substitution site and for the residue ($i + 1$) from that site. For these residues, we calculated $\Delta\Delta G_{HX}$ using the different k_{rc} values and eq 2. The solvent-exposed (Figure 5A) and buried (Figure 5B) Ala → Gly substitutions affect the stability of residues throughout the sequence of the protein. We have categorized the residues according to their ΔG_{HX} values in Table 4. If a residue exchanges from the globally unfolded form in both variants (solid bar), $\Delta\Delta G_{HX}$ for that residue approaches the $\Delta\Delta G_U$ value (hatched line). The average $\Delta\Delta G_{HX}$ value for these global residues is 0.72 ± 0.10 kcal/mol for the substitution at position 21 and -0.95 ± 0.02 kcal/mol for the substitution at position 23 (solid line). For residues where only one of the two variants has a global stability and the other is less stable (gray bars), the $\Delta\Delta G_{HX}$ values are also close to $\Delta\Delta G_U$. The less stable residues (open bars) are affected by mutation to varying amounts. Some of these residues have $\Delta\Delta G_{HX}$ values that are greater than $\Delta\Delta G_U$, while others are insensitive to the mutations in the helix.

DISCUSSION

Effect of Ala → Gly Substitutions on the Stability and the Structure of RNase T1. Alanine at position 21 is stabilizing by 1.0 kcal/mol compared to glycine as determined by the analysis of urea denaturation curves and 0.72 kcal/mol by hydrogen exchange. These values agree with those obtained previously in the G23A variants of RNase T1 (0.90 kcal/mol) and the peptides of identical sequence (0.98 kcal/mol) (*22*, *23*). The side chain at this position lies on the solvent-exposed surface of RNase T1 and has little contact with other residues. This is consistent with the observation that there are few changes in chemical shift for residues outside the helix. The stabilizing effect of alanine compared to glycine is caused primarily by the difference in helix propensities between the two amino acids (*43*). Alanine is a very good helix former, while glycine is entropically unfavorable because it lacks a β-carbon and hence can occupy a larger region of (Φ, Ψ) space in the unfolded state (*44*).

In contrast, alanine at position 23 is destabilizing by 1.1 kcal/mol compared to glycine by urea denaturation and by 1.0 kcal/mol by hydrogen exchange. This position in the helix is 100% buried according to the accessible surface area calculations of Lee and Richards (*45*) and packs tightly against the protein core. This is evident from the chemical shift and crystal structure differences between G23A and RNase T1 for residues in the helix and in the β-strands surrounding this site. These results show that the stability is reduced in G23A mainly because the additional methyl group introduces steric strain at the mutation site. This strain must be considerably larger than the helix stabilization expected for replacing glycine by alanine.

Most single site mutations in proteins do not significantly alter the NMR chemical shifts of residues throughout the structure; only residues near the mutation site are generally affected (see, for example, refs *13* and *46*−*48*). Interestingly, this has been seen even when introducing a charged residue into the hydrophobic core of thioredoxin (*49*). In this case, there are only significant chemical shift differences between the mutant (L78K) and the wild-type proteins for residues that are within 12 Å of the altered site. In our study, the A21G variants of RNase T1 display this typical behavior, while the G23A variants do not. We observe significant chemical shift changes for residues throughout the sequence when mutating a glycine to alanine at position 23 (Figures 2 and 3). Changes are even seen for residues in β-sheet 5 that are 20 Å away from the mutation site. Therefore, we decided to determine the X-ray structure to see if there was a major alteration in structure and found only minor differences (Figure 4). This is not always the case. For example, an A98V mutation in T4 lysozyme, where a bulkier side chain is introduced between two helices in the hydrophobic core of the C-terminal domain, shows large chemical shift changes (*50*) and structural rearrangements throughout the domain (*51*) (i.e., the helices move apart by up to 0.7 Å). The change in stability of the A98V mutation in T4 lysozyme is also much larger (4.9 kcal/mol) than is seen here for the G23A mutation in RNase T1.

We conclude that the NMR chemical shifts are very sensitive to the electronic environments of RNase T1 and the G23A variant, but only small perturbations in the structure and stability for this variant are observed. The results indicate that the G23A mutation transmits small changes throughout the entire structure. The results also show that since the chemical shift differences are greater for the mutations at site 23 than at site 21 and no major changes in structure for G23A mutation are seen, the structures of A21G and RNase T1 are likely identical.

Global Residues Determined by ΔG_{HX}. We observe a 2-fold difference in stability between the smallest and largest measurable ΔG_{HX} values for each variant (Table 4). Other amides in RNase T1, not included in Table 4, exchange much faster and have smaller ΔG_{HX} values. Hydrogen-bonding interactions and burial in the native state slow the exchange of many amide groups. Listed in Table 4 are the hydrogen bond acceptors of the protected amide groups in RNase T1. Almost all NH groups of these residues are hydrogen bonded in secondary and tertiary structures. The accessible surface area calculations show that the amide nitrogens of most residues that are protected from exchange are over 90% buried [except Ser12 (74%), Leu62 (77%), and Val89 (42.3%)] (*45*). The native-state structure does not, however, reveal why some residues have higher hydrogen-exchange stabilities than other residues. Protection from exchange in RNase T1, as in other proteins, has no clear correlation with the distribution of hydrogen bond distances, the *B*-factors from the crystal structure, or the temperature dependence of the amide proton chemical shifts by NMR (*52*, *53*).

The variation in stabilities for the slowly exchanging residues is likely explained by the unfolding process described by eq 1. The protein must unfold to some exchange competent form (intermediate or unfolded) before exchange occurs. The exchange of protected NH groups can be dominated by local fluctuations that break only a few hydrogen bonds rather than by global unfolding. Monitoring hydrogen exchange with an external perturbant can help decipher the exchange patterns of several higher energy partially unfolded forms under native-state conditions. For example, the dependence of ΔG_{HX} on denaturant (the *m*-value) can provide some clues to these processes.

A comparison of these types of experiments with pulse hydrogen-exchange studies suggest that the protection from exchange at equilibrium correlates with the order of protec-

tion of residues in the kinetic experiment (*4*, *16*, *18*). These results have led to the conclusion that protection from exchange may correlate with the folding pathway of a protein. Woodward and co-workers have suggested that the slowly exchanging hydrogens represent the protein folding core that determines the overall fold of the protein (*18* and references therein). The relationship between hydrogen exchange and the folding core is seen for RNase T1. Several of the slowest exchanging residues in β-sheets 2, 3, and 4 are protected first in the rapid-quench hydrogen-exchange experiment (*11*, *54*).

In the present study, we have focused mainly on global-exchanging residues since we did not monitor exchange as a function of an external perturbant. We identify global-exchanging residues under our experimental conditions by comparing ΔG_{HX} and ΔG^*_U. The residues with the largest ΔG_{HX} values for RNase T1 and the variants, boldfaced in Table 4, agree within error to the conformational stabilities measured by urea denaturation when the proline isomerization effect is taken into account.

Most of the global-exchanging residues in RNase T1 also exchange globally in the variants. This is seen for six residues (Trp59 and Phe80 may be included but could not be measured in all four variants.). Deviations in this trend are seen in the helix (Ala/Gly21, Gly/Ala23, and Tyr24), His40, His92, and two residues in sheets 3 and 4 (Arg77 and Ala87). The nonglobal stabilities for variants in this subset are just outside the error of the global stability except for residue 21 (refer to Table 4). These results may reflect the effects of the mutation. The most noticeable example is position 21. If a glycine is at position 21, a substantial decrease in ΔG_{HX} is seen compared to alanine at that position, suggesting a switch in exchange process from global to nonglobal.

The number of global-exchanging residues varies with the stability of RNase T1. Perturbants can strongly affect the stability of a protein, and the effect need not be the same for each residue. RNase T1 has fewer residues that exchange through the globally unfolded form at pD 5.6 and 25 °C, where the conformational stability is higher (~13 kcal/mol) than at higher temperatures (*11*) or pH 7 where the stability is 3−6 kcal/mol lower. At the most stable conditions, only the β-sheet residues (β-strands 2, 3, and 4) have ΔG_{HX} values that match ΔG^*_U, while residues in the helix have smaller ΔG_{HX} values. Under conditions where the protein is less stable, some residues in the helix (Gln20, Ala21, and Tyr24) now exchange globally, as seen here and by Mullins et al. (*11*) at temperatures greater than or equal to 40 °C. These results suggest that the helix in RNase T1 exchanges by nonglobal unfolding at very stable conditions and by a global process at lower conformational stabilities (~10 kcal/mol). Hilser et al. (*55*) have shown a similar trend for a fragment of λ repressor (residues [6−85]) using computer modeling.

Global Residues Determined by $\Delta\Delta G_{HX}$. The Ala → Gly substitutions at both positions 21 and 23 affect the stability of residues throughout the sequence by varying amounts as shown in Figure 5. Similar results have been seen for other single site mutations in thioredoxin (*49*), T4 lysozyme (*50*), and HPr (*48*). This is consistent with exchange of the most stable residues occurring from the globally unfolded ensemble. The residues that we define as global in Table 4 using the ΔG_{HX} criteria have $\Delta\Delta G_{HX}$ values close to $\Delta\Delta G_U$.

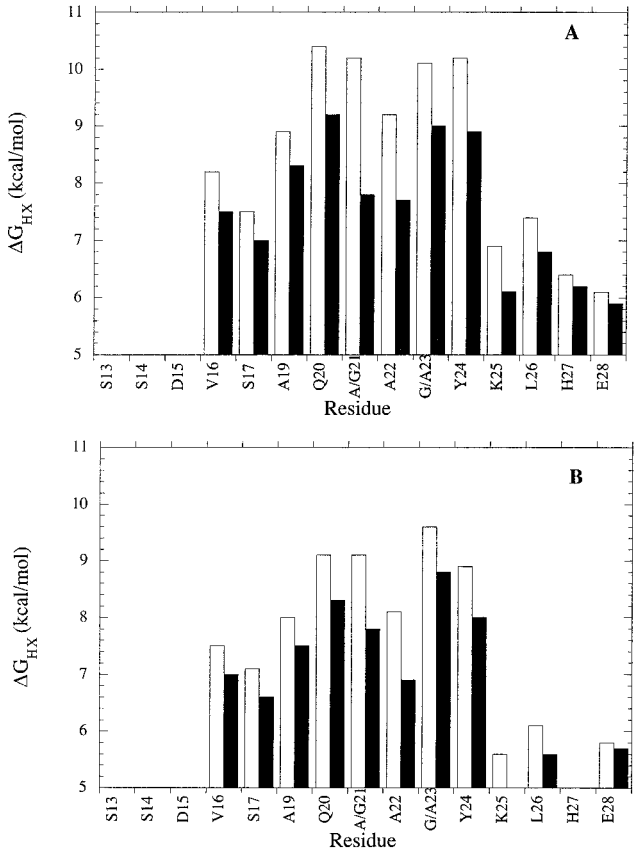

FIGURE 6: ΔG_{HX} values for the helical residues where position 23 is glycine (RNase T1 and A21G) (panel A) or alanine (G23A and A21G + G23A) (panel B). Open bars represent variants with an alanine at position 21, and closed bars represent variants with a glycine at position 21.

These residues of RNase T1 are located throughout the structure (Figure 1) and, by definition, must feel the full effect of the mutation. We find, however, that some residues with nonglobal ΔG_{HX} values also have $\Delta\Delta G_{HX}$ values near $\Delta\Delta G_U$. From our data alone, it is not possible to explain why these residues are strongly affected by mutation. Additional experiments monitoring the effect of an external perturbant on the hydrogen-exchange stabilities will be necessary to decipher the stability patterns of nonglobal residues. The results do show, however, that classifying global exchanging residues by examining only $\Delta\Delta G_{HD}$ upon mutation, as has been done for BPTI (*13*), may be deceiving.

Mutational analysis on CI2 (*15*) and barnase (*14*) shows results similar to those in this study: the ΔG_{HX} values for the most stable amide protons are similar to the ΔG_U value, and the $\Delta\Delta G_{HX}$ values for these residues are also close to the $\Delta\Delta G_U$ value. Unlike our results, Neira et al. (*15*) observed for CI2 that the majority of nonglobal residues are essentially not affected by the mutation. Perrett et al. (*14*) observe, however, for two stabilizing variants of barnase that some nonglobal residues have $\Delta\Delta G_{HX} \approx \Delta\Delta G_U$ (Table 6 in ref *14*), as is seen here for RNase T1. We conclude that global residues should be determined by comparing ΔG_{HX} and $\Delta\Delta G_{HX}$ upon mutation with conformational stabilities from traditional unfolding measurements (ΔG_U and $\Delta\Delta G_U$).

ΔG_{HX} and Helix Stability. The distribution of ΔG_{HX} values in the helix of RNase T1 and the variants is shown in Figure 6. The two panels show the effects of the Ala → Gly mutation at position 21 when position 23 is either glycine

(panel A) or alanine (panel B). The trend is essentially the same for the wild-type and the G23A RNase T1 backgrounds; the difference being the variants with glycine at position 23 are more stable. The trend in ΔG_{HX} values in the helix resembles those expected for a helical peptide in water with end fraying (*56*): the ΔG_{HX} values appear largest in the center of the helix (residues 20−24) and diminish at either end. The C-terminal residues are more stable than the N-terminal residues. The backbone amide protons of the first three N-terminal residues in the helix (Ser13, Ser14, and Asp15) exchange faster than can be detected probably because they lack backbone hydrogen-bond acceptors.

The $\Delta\Delta G_{HX}$ of the Ala → Gly substitution at position 21 is primarily caused by the difference in helix propensities between the two amino acids, as described above. If we look just at $\Delta\Delta G_{HX}$ values for the helical residues in Figure 5A, we observe that the largest stability change from the substitution is at the mutation site and Ala22. The destabilizing effect diminishes in the helix with distance from the substitution site. This result is independent of the identity of the residue at position 23 (Figure 6) and is similar to what is observed when substituting a helix-breaking residue like glycine in the center of an alanine-based peptide helix (*57*). We do not observe this trend when comparing the Ala → Gly variants at position 23 where the stability is not solely dependent upon helix propensity differences between alanine and glycine (Figure 5B).

Regardless, the Ala → Gly substitutions at position 21 or 23 have not destabilized the helix to the extent that it is not part of the global-exchanging core of the protein under our experimental conditions. At least one residue in the helix, Gln20, exchanges with global stability in all four variants.

Helix Propensity Difference between Ala and Gly at Site 21 in the Helix of RNase T1. The difference in helix propensities between alanine and glycine has been measured in various model systems, including α-helical peptides and proteins (for reviews, see *22*, *23*, and *43*). Most studies find a 1 kcal/mol difference in helix propensities between alanine and glycine. The two exceptions are found in the alanine-based AK/AQ (*58*) and EAK peptides (*59*). The effect of an Ala → Gly substitution in these peptides is closer to 2 kcal/mol. The alanine-based peptides contain multiple alanine residues, while other systems have more natural distributions of amino acids in their helical sequences. Recently, Luo and Baldwin (*60*) explain the discrepancy by showing that nonpolar side chains can shield the interaction between water and polar peptide groups in a side-chain-specific manner, thus, suggesting a context dependence of the helix propensity from neighboring residues in the sequence.

For either peptide or protein systems, the methods used to determine the free energy changes are model dependent. In peptide systems, the ellipticity values for each peptide containing the alanine or glycine substitution are converted to free energies by using helix-coil transition theories (*61*) to model the non-two-state nature of the overall transition. In protein backgrounds, the stability of the variant proteins is generally determined using urea denaturation, analyzed by the two-state unfolding model and the linear extrapolation method (*43*). Conversely, we use here an independent, model-free method, hydrogen exchange by NMR, to measure the stability difference between alanine and glycine variants in RNase T1. We examine directly the difference in rate constants to convert the data to $\Delta\Delta G_{HX}$. On average, the most stable residues show a 0.7 kcal/mol difference in stability for the Ala → Gly substitution at solvent-exposed position 21 in the RNase T1 helix. This is similar to the value of 1.0 kcal/mol determined by the two different model-dependent methods used in the same background sequence (*22*, *23*).

ACKNOWLEDGMENT

We thank Clare Woodward for a preprint of a recent review on hydrogen exchange, Kevin Shaw and Eric Hebert for help on molecular graphics, and members of the Pace and Scholtz laboratories for helpful discussions.

SUPPORTING INFORMATION AVAILABLE

One table containing the exchange rate constants (k_{ex}) for the four proteins. This material is available free of charge via the Internet at http://pubs.acs.org.

REFERENCES

1. Hvidt, A., and Neilson, S. O. (1966) *Adv. Protein Chem. 21*, 287−386.
2. Bai, Y., Milne, J. S., Mayne, L., and Englander, S. W. (1993) *Proteins 17*, 75−86.
3. Mayo, S. L., and Baldwin, R. L. (1993) *Science 262*, 873−876.
4. Bai, Y., Sosnick, T. R., Mayne, L., and Englander, S. W. (1995) *Science 269*, 192−197.
5. Chamberlain, A. K., Handel, T. M., and Marqusee, S. (1996) *Nat. Struct. Biol. 3*, 782−787.
6. Grantcharova, V. P., and Baker, D. (1997) *Biochemistry 36*, 15685−15692.
7. Yi, Q., Scalley, M. L., Simons, K. T., Gladwin, S. T., and Baker, D. (1997) *Folding Des. 2*, 271−279.
8. Bhuyan, A. K., and Udgaonkar, J. B. (1998) *Proteins 30*, 295−308.
9. Fuentes, E. J., and Wand, A. J. (1998) *Biochemistry 37*, 3687−3698.
10. Bai, Y., Milne, J. S., Mayne, L., and Englander, S. W. (1994) *Proteins 20*, 4−14.
11. Mullins, L. S., Pace, C. N., and Raushel, F. M. (1997) *Protein Sci. 6*, 1387−1395.
12. Fuentes, E. J., and Wand, A. J. (1998) *Biochemistry 37*, 9877−9883.
13. Kim, K.-S., Fuchs, J. A., and Woodward, C. K. (1993) *Biochemistry 32*, 9600−9608.
14. Perrett, S., Clarke, J., Hounslow, A., and Fersht, A. R. (1995) *Biochemistry 34*, 9288−9298.
15. Neira, J. L., Itzhaki, L. S., Otzen, D. E., Davis, B., and Fersht, A. R. (1997) *J. Mol. Biol. 270*, 99−110.
16. Chamberlain, A. K., and Marqusee, S. (1997) *Structure 5*, 859−863.
17. Krugelund, B. B., Heinemann, B., Knudsen, J., and Poulsen, F. M. (1998) *Protein Sci. 7*, 2237−2248.
18. Li, R., and Woodward, C. (1999) *Protein Sci. 8*, 1571−1591.
19. Neira, J. L., Sevilla, P., Menéndez, M., Bruix, M., and Rico, M. (1999) *J. Mol. Biol. 285*, 627−643.
20. Huyghues-Despointes, B. M. P., Scholtz, J. M., and Pace, C. N. (1999) *Nat. Struct. Biol. 6*, 210−212.
21. Reimer, U., Scherer, G., Drewello, M., Kruber, S., Schutkowski, M., and Fischer, G. (1998) *J. Mol. Biol. 279*, 449−460.
22. Myers, J. K., Pace, C. N., and Scholtz, J. M. (1997) *Proc. Natl. Acad. Sci. U.S.A. 94*, 2833−2837.
23. Myers, J. K., Pace, C. N., and Scholtz, J. M. (1997) *Biochemistry 36*, 10923−10929.
24. Myers, J. K., Smith, J. S., Pace, C. N., and Scholtz, J. M. (1996) *J. Mol. Biol. 263*, 390−395.

25. Landt, O., Grunert, H. P., and Hahn, U. (1990) *Gene 96*, 125−128.
26. Shirley, B. A., and Laurents, D. V. (1990) *J. Biochem. Biophys. Methods 20*, 181−188.
27. Pace, C. N. (1986) *Methods Enzymol. 131*, 266−280.
28. Glasoe, P. F., and Long, F. A. (1960) *J. Phys. Chem. 64*, 188−193.
29. Delaglio, F., Grzesiek, S., Vuister, G., Zhu, G., Pfeifer, J., and Bax, A. (1995) *J. Biomol. NMR 6*, 277−293.
30. Johnson, M. L., Correia, J. J., Yphantis, D. A., and Halvorson, H. R. (1981) *Biophysical J. 36*, 575−588.
31. McNutt, M., Mullins, L. S., Raushel, F. M., and Pace, C. N. (1990) *Biochemistry 29*, 7572−7576.
32. Schmidt, J., Thüring, H., Werner, A., Rüterjans, H., Quass, R., and Hahn, U. (1991) *Eur. J. Biochem. 97*, 643−653.
33. Hoffmann, E., and Rüterjans, H. (1988) *Eur. J. Biochem. 177*, 539−560.
34. CCP4. (1994) *Acta Crystallogr. 50*, 760−763.
35. Otwinowski, Z., and Minor, W. (1997) *Methods Enzymol. 276*, 307−326.
36. Zegers, I., Haikal, A. F., Palmer, R., and Wyns, L. (1994) *J. Biol. Chem. 269*, 127−133.
37. Brünger, A. T. (1992), Yale University, New Haven, Connecticut.
38. Laskowski, R. A., MacArthur, M. W., Moss, D. S., and Thornton, J. M. (1993) *J. Appl. Crystallogr. 26*, 283−291.
39. Berstein, F. C., Koetzle, T. F., Williams, G. B., Meyer, E. E., Brice, M. D., Rodgers, J. R., Kennard, O., Shimanouchi, T., and Tasumi, M. (1997) *J. Mol. Biol. 112*, 535−542.
40. Loris, R., Langhorst, U., De Vos, S., Decanniere, K., Bouchaert, J., Maes, D., Transue, T. R., and Steyaert, J. (1999) *Proteins 36*, 117−134.
41. Greene, R. F., and Pace, C. (1974) *J. Biol. Chem. 249*, 5388−5393.
42. Wells, J. A. (1990) *Biochemistry 29*, 8509−8517.
43. Pace, C. N., and Scholtz, J. M. (1998) *Biophys. J. 75*, 422−427.
44. Creamer, T. P., and Rose, G. D. (1994) *Proteins 19*, 85−97.
45. Lee, B., and Richards, F. M. (1971) *J. Mol. Biol. 55*, 379−400.
46. Thapar, R., Nicholson, E. M., Rajagopal, P., Waygood, E. B., Scholtz, J. M., and Klevit, R. E. (1996) *Biochemistry 35*, 11268−11277.
47. Lacroix, E., Bruix, M., López-Hernández, E., Serrano, L., and Rico, M. (1997) *J. Mol. Biol. 271*, 472−487.
48. Peterson, R. W., Nicholson, E. M., Thapar, R., Klevit, R. E., and Scholtz, J. M. (1999) *J. Mol. Biol. 286*, 1609−1619.
49. De Lorimier, R., Hellinga, H. W., and Spicer, L. D. (1996) *Protein Sci. 5*, 2552−2565.
50. Anderson, D. E., Lu, J., McIntosh, L., and Dahlquist, F. W. (1993) in *NMR of Proteins* (Clore, G., and Gronenborn, A., Eds.) pp 258−304, CRC Press, Boca Raton, FL.
51. Dao-pin, S., Alber, T., Baase, W. A., Wozniak, J. A., and Matthews, B. W. (1991) *J. Mol. Biol. 221*, 647−667.
52. Radford, S. E., Buck, M., Topping, K. D., Dobson, C. M., and Evans, P. A. (1992) *Proteins 14*, 237−248.
53. Milne, J. S., Roder, M. H., Wand, A. J., and Englander, S. W. (1998) *Protein Sci. 7*, 739−745.
54. Mullins, L. S., Pace, C. N., and Raushel, F. M. (1993) *Biochemistry 32*, 6152−6156.
55. Hilser, V. J., Dowdy, D., Oas, T. G., and Freire, E. (1998) *Proc. Natl. Acad. Sci. U.S.A. 95*, 9903−9908.
56. Scholtz, J. M., and Baldwin, R. L. (1995) in *Peptides: Synthesis, Structures, and Applications* (Gutte, B., Ed.) pp 171−192, Academic Press.
57. Chakrabartty, A., Schellman, J. A., and Baldwin, R. L. (1991) *Nature 351*, 586−588.
58. Rohl, C. A., Chakrabartty, A., and Baldwin, R. L. (1996) *Protein Sci. 5*, 2623−2637.
59. Park, S. H., Shalongo, W., and Stellwagen, E. (1993) *Biochemistry 32*, 7048−7053.
60. Luo, P., and Baldwin, R. L. (1999) *Proc. Natl. Acad. Sci. U.S.A. 96*, 4930−4935.
61. Lifson, R., and Roig, A. (1961) *J. Chem. Phys. 34*, 1963−1974.
62. Martinez-Oyanedel, J., Heineman, U., and Saenger, W. (1991) *J. Mol. Biol. 222*, 335−352.
63. Kraulis, P. J. (1991) *J. Appl. Crystallogr. 24*, 946−950.

BI9919450